Published in Surface Science 394, issues 1-3, 129-143, 1997
which should be used for any reference to this work

Structural and spectroscopic investigation of the Yb/Al(001) interface in the submonolayer coverage range

R. Fasel [a,*], P. Aebi [a], J. Osterwalder [b], L. Schlapbach [a]

[a] *Institut de Physique, Université de Fribourg, Pérolles, 1700 Fribourg, Switzerland*
[b] *Physik-Institut, Universität Zürich–Irchel, Winterthurerstr. 190, 8057 Zürich, Switzerland*

Abstract

The formation of submonolayer Yb overlayers on Al(001) has been studied by angle-scanned full-hemispherical X-ray photoelectron diffraction and angle-resolved ultraviolet photoelectron spectroscopy. It is shown that different phases, as observed by low-energy electron-diffraction, are formed up to a coverage of 0.5 ML where the first Yb layer is completed. An intimate connection of spectroscopic and structural properties is observed, reflected by marked changes of the Yb 4f core level spectra with increasing coverage. The surface Yb atoms are found to remain in the divalent $4f^{14}$ state for the full coverage range. Upon formation of $YbAl_3$-like nuclei at coverages above 0.5 ML, mixed valence of incorporated subsurface Yb atoms is observed, whereas the surface atoms persist in the divalent state

Keywords: Aluminium; Low energy electron diffraction (LEED); Metal–metal interfaces; Photoelectron diffraction; Surface electronic phenomena; Surface relaxation and reconstruction; Ultraviolet photoelectron spectroscopy; Ytterbium

1. Introduction

In the last 50 years, rare-earth metals and their intermetallic compounds have been studied extensively. There has been considerable interest in valence-fluctuation phenomena, and anomalous behavior of magnetic, electrical, thermal and structural properties have been attributed to a near degeneracy of the two electronic configurations $4f^n$ and $4f^{n+1}$ of the rare-earth ions [1]. There has also been an increasing interest in surface properties of the rare-earth metals, their compounds and quasi-two-dimensional overlayers. Many phenomena are connected with the loss of symmetry and the related change in coordination of atoms at the surface. Coordination-dependent core-level binding-energy shifts [2], surface valence transitions [3], surface relaxations and reconstructions [4] have been reported.

Owing to their mixed-valence behavior, Yb–Al intermetallic compounds have been the object of many studies. Yb, which in the metallic state is divalent with a filled 4f shell, is found in both divalent $4f^{14}$ and trivalent $4f^{13}$ states in Yb–Al compounds. In the $YbAl_2$ and $YbAl_3$ bulk systems the valence fluctuates between the divalent and trivalent configurations [5,6], whereas their surfaces are reported to remain in the divalent state [6–8]. For mixed-valence Yb–Al thin films divalent

* Corresponding author. Present adress: La Trobe University, School of Physics, Faculty of Science and Technology, Bundoora, Vic. 3083, Australia. Fax: (+61) 3 9479 1552; e-mail: roman.fasel@latrobe.edu.au

surface Yb atoms are reported as well, whereas a mixed-valence state is found at elevated temperatures where interdiffusion takes place [9]. Thin films of Yb overlayers on Al(110) have also been studied, and a divalent surface layer has been reported [10]. From a study of the interface of Yb on polycrystalline Al a strong Yb contraction within the first monolayer has been determined, indicating the occurrence of a mixed-valence behavior of Yb on Al [11].

However, the interpretation of spectroscopic data has often remained vague owing to a lack of information concerning the surface structure. In this paper, structural and spectroscopic results from the Yb/Al(001) interface for submonolayer Yb coverages are reported. Different structural phases have been observed and characterized by low-energy electron-diffraction (LEED) and X-ray photoelectron diffraction (XPD). By measuring ultraviolet photoelectron spectra from these different phases, the interplay of electronic and structural properties has been investigated with particular attention to the occurrence of mixed valence.

2. Experimental

The experiments were performed in a VG Escalab Mark II spectrometer modified for motorized sequential angle-scanning data acquisition, and with a working pressure in the lower 10^{-11} mbar region. X-ray photoelectron spectra and diffraction patterns were measured using Si Kα ($h\nu = 1740$ eV) radiation, which allowed the excitation of the Yb 3d and Al 1s core levels. The ultraviolet photoelectron spectroscopy (UPS) measurements were performed with unmonochromatized He I ($h\nu = 21.2$ eV) and He II ($h\nu = 40.8$ eV) radiation from a discharge lamp. For the UPS measurements the analyzer was operated with an energy resolution of 50 meV. All experiments were performed at room temperature. Contamination-free surfaces were prepared by a combination of Ar^+ sputtering and annealing at 500°C. Yb was evaporated from a resistively heated stainless steel crucible onto the substrate which was kept at room temperature. During Yb deposition the pressure was in the lower 10^{-10} mbar range. The evaporations were performed at rates below 0.05 ML min^{-1}, with 1 ML corresponding to one Yb atom per surface Al atom. The purity of the deposited Yb layers, as well as the coverage, was checked by core-level photoemission. Coverages are given in monolayers. Before and after Yb deposition, long-range order of the surface was probed by LEED.

3. Results and discussion

3.1. Surface atomic structure

3.1.1. Yb deposition at room temperature

Depending on the Yb coverage of the surface, different ordered phases are observed by LEED (Fig. 1). Up to a coverage of about 0.1 ML, the LEED pattern reveals the (1×1) periodicity of the Al(001) surface. Already for slightly higher coverages, the pattern shown in Fig. 1a starts to develop. With increasing coverage, the overlayer spots of this pattern get sharper and the initially diffuse background intensity disappears, until at a coverage of 0.2 ML the maximum sharpness is reached (Fig. 1a). The periodicity corresponding to this LEED pattern is $(\sqrt{5} \times \sqrt{5})R \pm 26.6°$ (Fig. 1g), and the surface thus consists of two domains rotated by $\pm 26.6°$ with regard to a close-packed direction of the Al(001) surface layer. According to the Yb coverage of 0.2 ML where this $(\sqrt{5} \times \sqrt{5})R \pm 26.6°$ LEED pattern is most clearly observed, each $\sqrt{5} \times \sqrt{5}$ unit cell contains exactly one Yb atom.

Between 0.2 ML and 0.25 ML of Yb coverage, a discontinuous phase transition is observed: within this narrow coverage regime, the LEED pattern changes from $(\sqrt{5} \times \sqrt{5})R \pm 26.6°$ to the one shown in Fig. 1b, which reveals different periodicity. When the coverage is further increased, this pattern continuously transforms into a $c(2 \times 2)$ pattern with sharp overlayer spots at a coverage of 0.5 ML (Fig. 1c–f). Upon increasing the coverage from 0.25 ML to 0.5 ML, the four overlayer spots centered around the $(\frac{1}{2}, \frac{1}{2})$ position in the pattern of Fig. 1b become diffuse and move

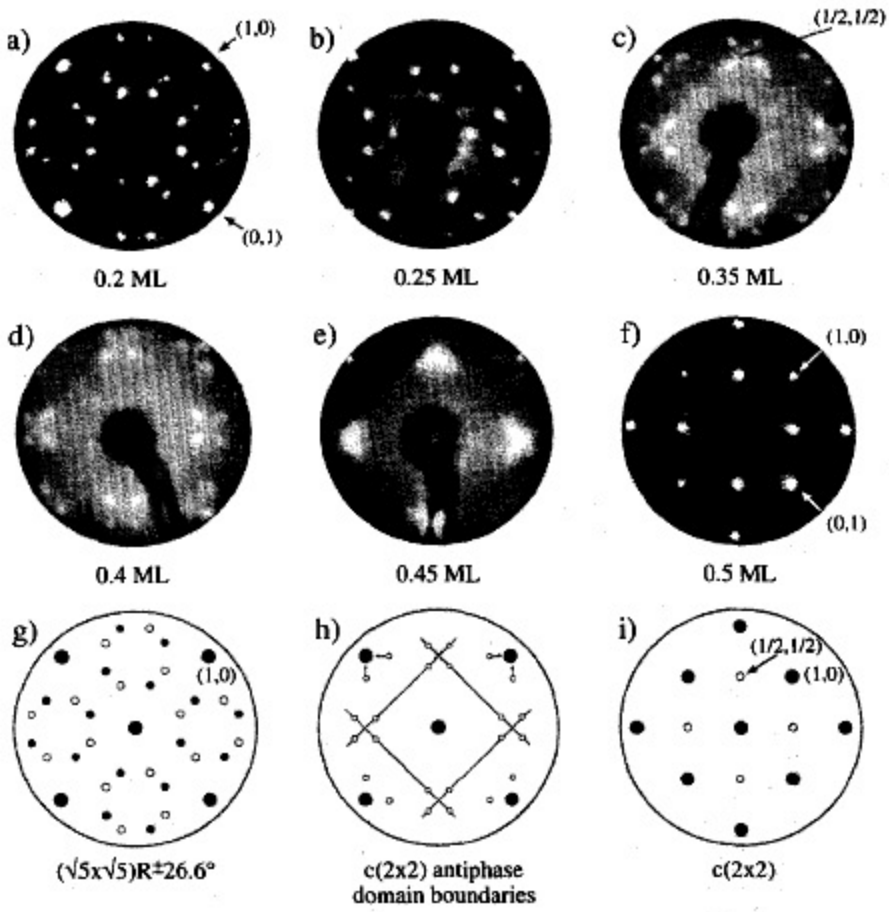

Fig. 1. LEED patterns observed upon formation of submonolayer Yb overlayers on Al(001). The energies of the LEED patterns are (a) 46 eV, (b) 36 eV, (c) 34 eV, (d) 34 eV, (e) 32 eV and (f) 83 eV. A schematic representation of the observed LEED patterns is given in (g), (h) and (i). The overlayer spots corresponding to the two different domains of the $(\sqrt{5}\times\sqrt{5})R\pm26.6°$ overlayer are given by filled and open small circles. In (h), the displacement of the overlayer spots with increasing coverage is indicated by arrows.

towards the half-order $(\frac{1}{2}, \frac{1}{2})$ position, while the spots close to the $(1, 0)$ positions move towards the first order $(1, 0)$ substrate beams (Fig. 1h). This indicates that the patterns in Fig. 1b–e can be understood as split $c(2\times2)$ patterns, with the splitting gradually reducing as the coverage approaches 0.5 ML (Fig. 1h,i). Furthermore, a broadening of the spots is observed along diagonal lines during this transition, which indicates the presence of statistical disorder. An alternative interpretation of the transition observed in Fig. 1b–f is that the Yb overlayer has a continuously changing surface net dimension, with the surface unit vectors continuously changing in length as well as in direction with increasing coverage. This interpretation, however, is not consistent with the photoelectron diffraction results presented below and will, therefore, not be discussed further.

The diffraction patterns from random $c(2\times2)$ nuclei and parallel arrays of antiphase domain boundaries in the $c(2\times2)$ surface structure have been simulated by Ellis [12]. The results of these simulations look very much like the LEED patterns in Fig. 1b–e: discrete antiphase splitting as in Fig. 1b appears when there is ordering of the domains, either into approximately equally spaced parallel arrays, or into rectangular regions of approximately equal size with a predominance of

90° intersections. As the domain size increases, the four split spots contract towards the corresponding integer- or half-order spots, and finally a sharp $c(2\times2)$ pattern is obtained for domains larger than a critical size. These simulations thus very nicely explain the nature of the phase transition observed between 0.2 ML and 0.5 ML of Yb coverage: when the Yb coverage exceeds the critical coverage of 0.2 ML corresponding to the $(\sqrt{5}\times\sqrt{5})R\pm26.6°$ phase, the surface converts into a regular array of $c(2\times2)$ nuclei, where the nuclei are considerably out of phase with the neighboring ones. For this ordered arrangement of very small $c(2\times2)$ domains (large splitting of the half-order spots) the LEED pattern of Fig. 1b is observed. With increasing coverage, the individual $c(2\times2)$ domains become larger and the four split spots therefore move together (Fig. 1c–e). Some domains grow faster than others, which leads to a superposition of the corresponding split spots and, therefore, to a linear broadening, as observed in the LEED patterns.

At the coverage of 0.5 ML, a sharp $c(2\times2)$ LEED pattern is observed (Fig. 1f); this indicates that the individual $c(2\times2)$ domains are now larger than the transfer width of the LEED experiment, which is of the order of 100 Å. For coverages higher than 0.5 ML, this $c(2\times2)$ LEED pattern gradually disappears, and at about 0.8 ML it can no longer be distinguished from the diffuse background. Therefore, above 0.5 ML the Yb/Al(001) interface appears to be disordered, at least on a scale of the order of a few tens of $(Å)^2$.

Whereas the LEED patterns discussed above reflect the degree of long-range order and the periodicity present on the surface, XPD [13] pat-

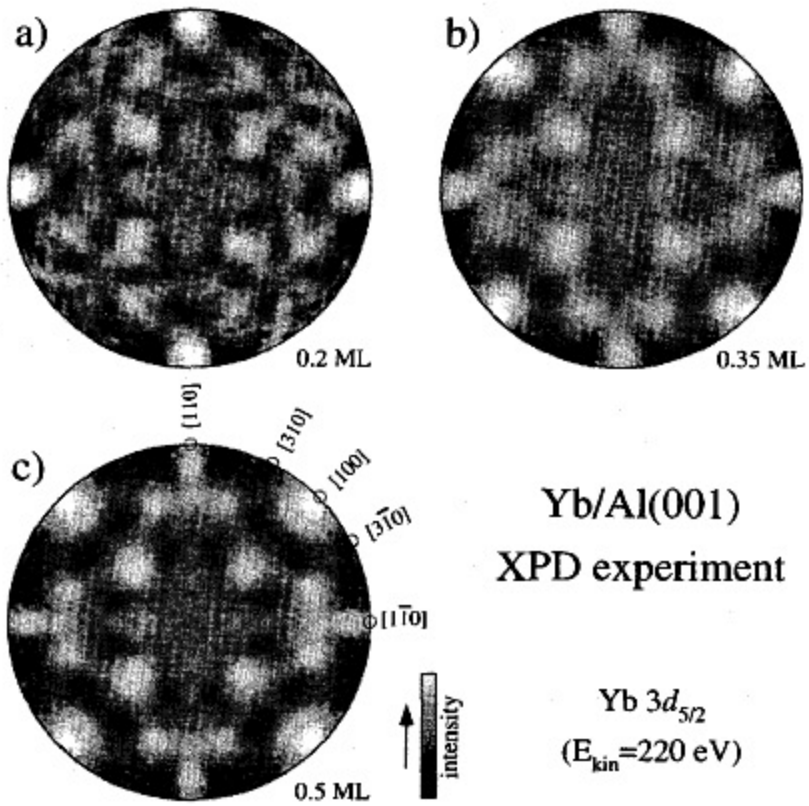

Fig. 2. Experimental Yb $3d_{5/2}$ XPD pattern (a) from the 0.2 ML $(\sqrt{5}\times\sqrt{5})R27°$ structure, (b) the 0.35 ML $c(2\times2)$ antiphase domain boundary structure, and (c) the 0.5 ML $c(2\times2)$ structure. The orientation of the substrate surface which is valid for all measurements is indicated in (c).

terns from adsorbate emitters are mainly sensitive to the very local order around the adsorbate atoms [14–17]. At electron kinetic energies above about 200 eV, the strongly anisotropic scattering of the photoelectrons by the ion cores leads to a forward focusing of electron flux along the emitter–scatterer axis. Prominent intensity maxima in full-hemispherical XPD patterns can, therefore, often be identified with bond directions. One finds that the photoelectron angular distribution is, to a first approximation, a forward-projected image of the atomic structure around the photoemitter. Analysis of the symmetry and positions of forward-focusing maxima permit a very straightforward structural interpretation of XPD data [15,16]. LEED and XPD, therefore, yield quite complementary information, and a more detailed picture of the ordered phases and phase transitions observed by LEED might be gained by XPD.

The Yb $3d_{5/2}$ XPD patterns from $(\sqrt{5}\times\sqrt{5})$R26.6°-Yb/Al(001), from the c(2×2) antiphase domain boundary structure at 0.35 ML of Yb coverage and from c(2×2)-Yb/Al(001) are shown in Fig. 2. To maximize the statistical accuracy the patterns have been azimuthally averaged by exploiting the fourfold rotational symmetry of the systems. To eliminate the smooth polar angle dependence of the photoelectron intensity typical for adsorbate emission, the patterns have been normalized with respect to the mean intensity for each polar emission angle. The data are given in stereographic projection and in a linear gray scale with maximum intensity (1.13) corresponding to white and minimum intensity (0.92) to black. The same scale has been used for the three patterns. The center of each plot represents normal emission, and the outer ring corresponds to grazing emission along the surface plane.

A common feature of the diffraction patterns of Fig. 2 is that the strongest anisotropy is observed at very grazing emission angles along the surface plane. For the $(\sqrt{5}\times\sqrt{5})$R26.6° structure, four prominent maxima are observed along the [110] directions (Fig. 2a), whereas the patterns from the domain boundary and the c(2×2) structures (Fig. 2b,c) exhibit prominent maxima along the [100] directions. The absence of intensity maxima along the [100] directions and the observation of four dominant intensity enhancements along the [110] directions in the $(\sqrt{5}\times\sqrt{5})$R26.6° pattern are not compatible with on-surface Yb adsorption sites, but indicate strongly the occupancy of substitutional sites. We have previously shown [18] that the $(\sqrt{5}\times\sqrt{5})$R26.6°-Yb/Al(001) structure indeed consists of Yb atoms adsorbed in substitutional sites where every fifth surface Al atom has been removed (Fig. 3). The residual first layer Al atoms have been found to be displaced laterally by more than 0.5 Å from their bulk position, resulting in a quasi-eightfold coordination of Yb within the first layer. We have, furthermore, shown that small unreconstructed surface patches coexist with the long-range ordered $(\sqrt{5}\times\sqrt{5})$R26.6° reconstruction, and that these patches contain about 0.03 ML of Yb atoms in second layer Al sites [18]. The presence of these subsurface Yb atoms leaves a

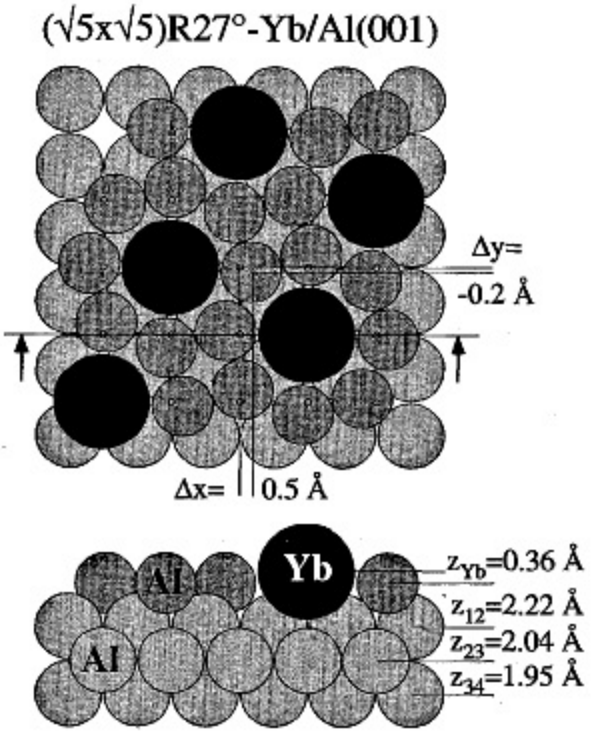

Fig. 3. Structural model of $(\sqrt{5}\times\sqrt{5})$R26.6°-Yb/Al(001) as determined by XPD and LEED [18]. The Yb atoms are adsorbed in substitutional sites, and the remaining top-layer Al atoms are displaced laterally from their bulk position by more than 0.5 Å.

clear fingerprint in the diffraction pattern of Fig. 2a: the four intensity maxima observed at 45° polar emission angle in the ⟨100⟩ azimuths are due to photoelectrons emitted from these second layer Yb atoms which are forward-focused by the surface Al atoms.

A comparison of the 0.35 ML antiphase domain boundary XPD pattern (Fig. 2b) and the 0.2 ML $(\sqrt{5}\times\sqrt{5})$R26.6° pattern (Fig. 2a) demonstrates that a drastic change in the local order occurs between these two coverages. Interestingly, the XPD patterns in Figs. 2b and c, however, are almost identical, irrespective of the different Yb coverage and the different corresponding LEED patterns. From this observation it can immediately be concluded that the average local Yb environment in the 0.35 ML Yb/Al(001) system is the same as in the 0.5 ML c(2×2)-Yb/Al(001) structure. In fact, the same XPD pattern is observed for the entire coverage regime between 0.25 ML and 0.5 ML where the continuous contraction of the split spots is observed by LEED. This represents further evidence that the surface already consists of c(2×2) nuclei at coverages as low as 0.25 ML which grow in size with increasing coverage. The close similarity of the diffraction anisotropies (Table 1) from the 0.35 ML antiphase domain boundary structure and the 0.5 ML c(2×2) structure compared with the significantly different anisotropies from the 0.2 ML $(\sqrt{5}\times\sqrt{5})$R26.6° structure indicates strongly that the surface already consists entirely of c(2×2) nuclei at 0.35 ML coverage. This, and the fact that the LEED pattern from the 0.25 ML surface shows no residual features characteristic of the 0.2 ML $(\sqrt{5}\times\sqrt{5})$R26.6° pattern, indicates that a collective rearrangement of the entire surface is induced by adsorption of as little as 0.05 ML of Yb onto the $(\sqrt{5}\times\sqrt{5})$R26.6° structure.

Table 1
Anisotropy of prominent forward-focusing maxima observed in the XPD patterns from the 0.2 ML $(\sqrt{5}\times\sqrt{5})$R26.6° structure (Fig. 2a), the 0.35 ML antiphase domain boundary structure (Fig. 2b), and the 0.5 ML c(2×2) structure (Fig. 2c)

Direction	Anisotropy (%)		
	0.2 ML	0.35 ML	0.5 ML
[110]	19	10	9
[100]	0	16	16
[101]	7	6	6

As is the case in the $(\sqrt{5}\times\sqrt{5})$R26.6° XPD pattern (Fig. 2a), four intensity maxima at a 45° polar emission angle in the ⟨100⟩-type azimuths ([101]-type directions) are observed in the c(2×2) pattern (Fig. 2c) as well as in the c(2×2) antiphase domain boundary pattern (Fig. 2b). These intensity maxima represent a fingerprint of second-layer Yb atoms [18], and it can thus be concluded that the subsurface Yb atoms persist across the phase transition from the $(\sqrt{5}\times\sqrt{5})$R26.6° to the c(2×2) structure. Whether the surface patches containing subsurface Yb atoms finally get covered by c(2×2) domains cannot be decided from the present analysis.

For the c(2×2) and c(2×2) antiphase domain boundary structures it can be concluded from the XPD patterns of Fig. 2 that the Yb atoms are definitely not coplanar with the topmost Al atoms. The only configuration that might result in a coplanar Yb–Al layer would be the substitutional c(2×2) geometry. In this geometry, however, the substitutional Yb atoms have coplanar Al nearest-neighbors along the [110] directions. These Al atoms would forward-focus the Yb 3d photoelectrons and give rise to dominant forward-scattering maxima along the [110] directions, which are not observed in Fig. 2b,c. Whether the Yb atoms in the c(2×2) and c(2×2) antiphase domain boundary structures are adsorbed in on-surface sites or—with a considerable buckling—in substitutional sites, as in the lower coverage $(\sqrt{5}\times\sqrt{5})$R26.6° phase, cannot be decided from the present data. The large size of the Yb atoms is expected to result in a large vertical separation of Yb and Al in these structures, which leads to Yb 3d diffraction patterns dominated by Yb–Yb intralayer scattering. Since the Yb–Al scattering anisotropies are relatively weak in this case, a quantitative data analysis has not been attempted here. It must be noted that, owing to the extremely high reactivity of these systems, the collection of high-quality XPD data resolving the weak Yb–Al scattering anisotropies is limited by measuring time.

3.1.2. *Influence of substrate temperature: interdiffusion and segregation*

We have previously shown [18] that at room temperature the $(\sqrt{5}\times\sqrt{5})$R26.6°-Yb/Al(001) interface already contains Yb atoms which have diffused into the second substrate layer. To investigate the effect of substrate temperature on the structure of the overlayer, Yb films of different coverages ranging from 0.2 ML up to several monolayers have been annealed to 450°C for 15 min and analyzed after cooling to room temperature. Independently of the starting coverage, a $(\sqrt{5}\times\sqrt{5})$R26.6° LEED pattern has always been obtained from these annealed samples, and the final coverage, as determined by XPS, has always been 0.2 ± 0.02 ML. Furthermore, the XPD patterns from all annealed samples have been found to be identical to the one from the room-temperature $(\sqrt{5}\times\sqrt{5})$R26.6° structure shown in Fig. 2a; therefore, it can be concluded that the same surface structure is formed upon annealing a Yb film of coverage >0.2 ML and upon room-temperature deposition of 0.2 ML of Yb. This structure thus represents the most stable adsorption geometry of Yb on Al(001).

In order to settle the question of whether the effect of the annealing procedure is to desorb the Yb atoms in excess of 0.2 ML or it is the diffusion of Yb into the substrate that takes place, a several monolayers thick Yb film has been annealed slowly up to 510°C and continuously analyzed by XPS and thermal desorption spectroscopy during this process. No signal related to Yb could ever be detected in the mass spectrometer during these annealing cycles. It must, therefore, be concluded that interdiffusion rather than desorption takes place. This is also confirmed by the fact that when the Yb atoms forming the $(\sqrt{5}\times\sqrt{5})$R26.6° surface structure are removed by a brief sputtering and the substrate is subsequently annealed to 400°C, the Yb that had diffused into the Al substrate segregates to the surface and the same $(\sqrt{5}\times\sqrt{5})$R26.6° structure is recovered.

The ratio of the Yb $3d_{5/2}$ and Al 1s intensities measured during the annealing procedure described above is plotted as a function of substrate temperature in Fig. 4. The data points are

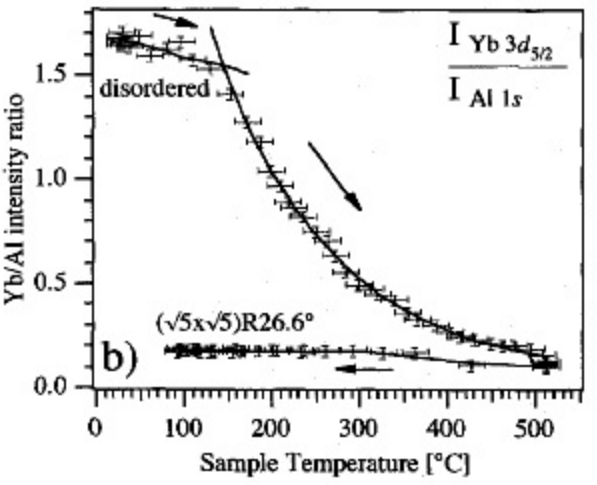

Fig. 4. Ratio of the Yb $3d_{5/2}$ and Al 1s photoelectron intensities measured during an annealing cycle from room temperature to 520°C and subsequent cooling to room temperature. The initial coverage of the sample has been several monolayers, and after the heat treatment a stable Yb surface layer of 0.2 ML coverage is obtained. The several monolayers thick Yb overlayer, which is structurally disordered, is found to transform into a well-ordered $(\sqrt{5}\times\sqrt{5})$R26.6° overlayer of coverage 0.2 ML by diffusion of Yb into the Al substrate. The diffusion occurs in two steps: a slow diffusion is observed at temperatures up to about 140°C, and a strongly enhanced diffusion occurs for higher temperatures.

equally spaced in time: spectra have been taken every 2.5 min. The diffusion of Yb into the Al substrate is found to take place in two steps (Fig. 4): a slow diffusion with a roughly linear decrease of the Yb–Al intensity ratio is observed up to a substrate temperature of about 140°C, and a strongly enhanced diffusion occurs as the temperature is further increased. In this temperature range, an exponential decrease of the Yb–Al intensity ratio is observed. The intensity ratio curve in Fig. 4 finally levels off at a ratio of 0.13, and upon cooling to room temperature a slight increase to about 0.18 is observed. This slight increase with decreasing temperature might be due to the increasing Debye–Waller factor or/and to surface segregation of Yb atoms diffused into the Al substrate.

A very similar behavior has been observed by Onsgaard et al. [19] for the Yb/Al(110) interface. As in the present case, a slow diffusion of Yb into the Al substrate has been found for temperatures

close to room temperature, and a strongly enhanced diffusion for temperatures around 300°C. The initially slow diffusion has been rationalized by the existence of a potential barrier at the selvedge [19]. We propose that this potential barrier arises from the energy needed to promote a 4f electron to the conduction band. We have shown in Ref. [20] that Yb atoms located in the second layer of the Al(001) substrate are in a mixed-valence $4f^{14-\delta}$ state, which is also the case for Yb in $YbAl_2$ and $YbAl_3$. On the other hand, the Yb/Al(001) interface consists of divalent $4f^{14}$ Yb, (see below) and metallic Yb is also purely divalent. To penetrate the top substrate layer, the Yb atoms therefore have to promote a 4f electron partly to the conduction band.

At first glance, the occurrence of mixed-valence second-layer Yb atoms already in the room-temperature $(\sqrt{5}\times\sqrt{5})$R26.6° structure [18,20] seems to be in contradiction with the above explanation. However, there is an alternative scenario for the incorporation of subsurface Yb atoms in this phase. It can be expected that in the initial stage of Yb deposition the Yb atoms will preferentially adsorb at defects and steps where they find maximum coordination. The formation of the $(\sqrt{5}\times\sqrt{5})$R26.6° structure involves the removal of 0.2 ML of surface Al atoms. It can be assumed that the ejected Al atoms diffuse across the surface until they can be re-adsorbed on a favorable site, e.g. a defect or a step. Instead of having penetrated the top surface layer, the subsurface Yb atoms may, therefore, be those adsorbed in the initial nucleation process and subsequently buried by Al atoms removed from the surface upon formation of the $(\sqrt{5}\times\sqrt{5})$R26.6° phase. Apart from the fact that this scenario seems to be favored by energetic reasons, it is also consistent with the observation of 0.03 ML of subsurface Yb atoms coexisting with the $(\sqrt{5}\times\sqrt{5})$R26.6° structure [18]. The 0.17 ML of Yb atoms in the reconstructed $(\sqrt{5}\times\sqrt{5})$R26.6° phase cover 85% of the total surface area, and the 0.03 ML of subsurface Yb atoms are thus distributed over the remaining 15% surface area. The amount of 0.17 ML of Al atoms removed from the top substrate layer upon formation of the substitutional $(\sqrt{5}\times\sqrt{5})$R26.6° structure corresponds nicely to the number of atoms needed to cover and bury the 15% surface area already occupied by Yb atoms adsorbed in the initial nucleation process.

A schematic phase diagram of the submonolayer Yb/Al(001) system derived from the present results is shown in Fig. 5. At room temperature, the $(\sqrt{5}\times\sqrt{5})$R26.6° structure is formed for coverages between 0.15 ML and 0.2 ML. This phase is stable up to near the melting temperature of 660°C of Al. Between 0.2 ML and 0.25 ML, a discontinuous transition from the $(\sqrt{5}\times\sqrt{5})$R26.6° structure to a phase consisting of a regular arrangement of $c(2\times2)$ nuclei occurs. With increasing coverage these $c(2\times2)$ nuclei grow in size, and the phase observed between 0.25 ML and 0.5 ML consists of $c(2\times2)$ domains of different sizes which are out of phase with each other. In a very narrow coverage regime around 0.5 ML, a well-ordered $c(2\times2)$ phase is observed, which gradually disorders when the coverage is further increased above 0.5 ML. For higher temperatures, the surface converts irreversibly, and irrespective of the initial Yb coverage, to the stable $(\sqrt{5}\times\sqrt{5})$R26.6° structure, and the

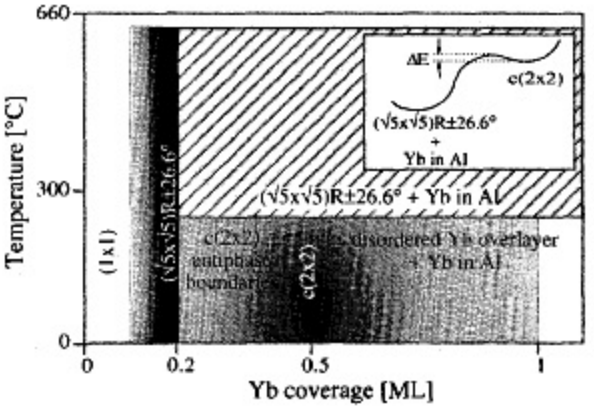

Fig. 5. Schematic phase diagram of the submonolayer Yb/Al(001) system. The degree of adsorbate long-range order is given in a gray-scale representation, with well-ordered regions in black and disordered regions in white. For temperatures above 200°C, the Yb in excess of the 0.2 ML forming the stable $(\sqrt{5}\times\sqrt{5})$R26.6° surface layer is found to diffuse into the substrate. The inset shows a schematic energy diagram: at higher substrate temperatures the potential barrier ΔE for diffusion of Yb into the substrate can be overcome, and the metastable $c(2\times2)$ structure transforms into the stable $(\sqrt{5}\times\sqrt{5})$R26.6° structure.

Yb in excess of the 0.2 ML forming the $(\sqrt{5}\times\sqrt{5})$R26.6° surface structure is found to diffuse into the Al substrate.

3.2. *Surface electronic structure*

3.2.1. *The Yb 4f spectrum*

The He I excited normal emission photoelectron spectra in the energy region from the Fermi level to 3.5 eV binding energy are shown in Fig. 6 for different Yb coverages. The spectra of Fig. 6a–g correspond to gradually increasing Yb coverage from 0.2 ML to 0.7 ML, and the spectrum in Fig. 6h has been obtained for a film of approximately 2 ML of Yb. The spectrum in Fig. 6a from the $(\sqrt{5}\times\sqrt{5})$R26.6° phase shows three peaks at 1.00 eV, 2.27 eV and 2.88 eV below the Fermi level. The first two peaks at 1.00 eV and 2.27 eV are due to Yb 4f emission, which occurs as a doublet separated by 1.27 eV due to the spin–orbit interaction. The additional peak labeled S is due to the sp surface state of the Al(001) surface and will be discussed in Section 3.2.2.

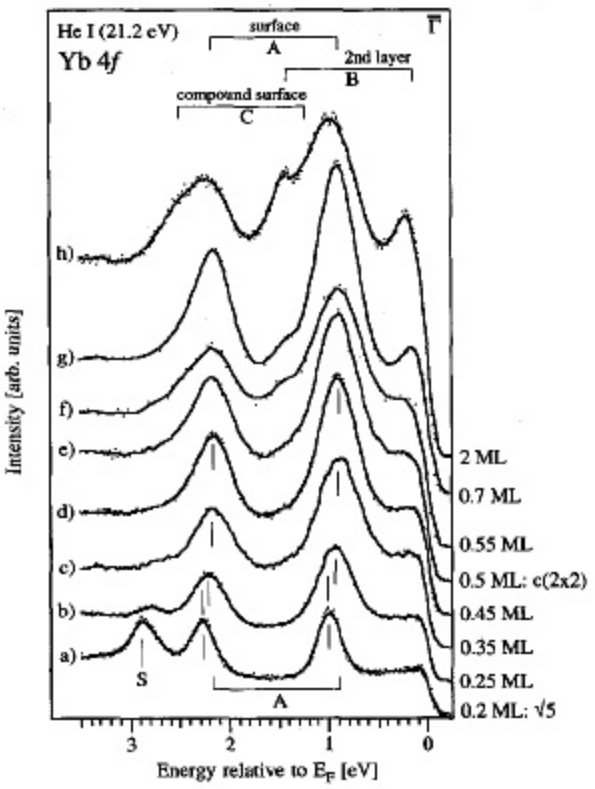

Fig. 6. He I excited valence-band photoemission spectra of Yb overlayers on Al(001). The different spectra correspond to Yb coverages of (a) 0.2 ML, (b) 0.25 ML, (c) 0.35 ML, (d) 0.45 ML, (e) 0.5 ML, (f) 0.55 ML, (g) 0.7 ML and (h) ≈2 ML. The features labeled A, B and C are assigned to the Yb $4f_{7/2,5/2}$ components of Yb at the Yb/Al interface, of Yb in a surrounding of Al ($YbAl_3$-like nuclei) and of Yb at the surface of the growing $YbAl_3$-like nuclei. The additional peak labeled S visible in the first two spectra is due to a zone-center surface state, as discussed in the text. Note the large shift of 70 meV of the peaks A between spectrum (a) and spectrum (b) which correspond to 0.2 ML and 0.25 ML respectively.

The structural phase transition from the $(\sqrt{5}\times\sqrt{5})$R26.6° phase to the c(2×2) antiphase domain boundary phase between 0.2 ML and 0.25 ML is clearly reflected in the Yb 4f spectra from the respective samples. The spectrum in Fig. 6b has been obtained from the 0.25 ML sample which showed the LEED pattern of Fig. 1b. The Yb 4f peaks in the Fig. 6b are shifted by 0.07 eV towards lower binding energy with respect to the position in Fig. 6a, and a considerable broadening is observed. The surface state peak S is suppressed strongly and is shifted slightly to lower binding energies. A further shift of the Yb 4f peaks of 0.02 eV is observed in the spectrum in Fig. 6c, which corresponds to 0.35 ML coverage, and the 0.45 ML spectrum in Fig. 6d again shows a shift of 0.01 eV towards the Fermi level. For the c(2×2) phase at 0.5 ML, the $4f_{7/2}$ peak is observed at a binding energy of 0.9 eV (Fig. 6e). For higher coverages of 0.55 ML and 0.7 ML, where the surface gradually disorders, no further shift of this 4f doublet A is observed (Fig. 6f,g). As is already weakly seen in Fig. 6e from the c(2×2) phase, an additional doublet B at 0.12 eV and 1.39 eV binding energy grows for coverages higher than 0.5 ML. In Fig. 6h from the 2 ML film, this doublet B is most clearly recognized. In this spectrum, a third doublet C with peaks at about 1.22 eV and 2.49 eV binding energy accounts for the much larger line widths of doublet A.

From the coverage dependence of these spectra, an assignment of the peaks A, B and C can be made as follows. The doublet labeled A is clearly due to the Yb–Al interface. Its location far below the Fermi level shows that the Yb–Al interface

consists of divalent $4f^{14}$ Yb. During the structural transition from the 0.2 ML $(\sqrt{5}\times\sqrt{5})R26.6°$ phase to the 0.5 ML $c(2\times2)$ phase the doublet A shifts by 0.1 eV to lower binding energies. The Yb $4f_{7/2}$ binding energies, of 1.00 eV and 0.90 eV in the $(\sqrt{5}\times\sqrt{5})R26.6°$ and $c(2\times2)$ structures respectively, are slightly lower than the binding energies of the divalent surface components in $YbAl_3$ and $YbAl_2$. Kaindl et al. [7] determined the Yb $4f_{7/2}$ components in $YbAl_2$ to be at 1.16 eV, 0.58 eV and 0.24 eV for the first and second surface layers and the bulk respectively. For $YbAl_3$, Patthey et al. [6] gave values of 1.2 eV and 0.24 eV for the surface and bulk components respectively, whereas a slightly different value of about 1 eV for the surface component can be read from the measurements of Oh et al. [8]. It must be noted that the measurements on these Yb–Al intermetallic compounds have been performed on polycrystalline samples, which leads to much broader (>0.7 eV) surface peaks than observed in the present case (0.3–0.45 eV). Therefore, the values given above have to be taken as average values over different surface facets. A $4f_{7/2}$ binding energy of about 1.1 eV was found for the divalent surface layer formed upon deposition of Yb on Al(110) [21], which is slightly larger than the values determined in the present study. It is also interesting to compare the energy positions of the 4f peaks with those obtained from Yb metal. Schneider et al. [2] determined multiple surface shifts due to different coordination numbers of the surface atoms. Binding energies of the Yb $4f_{7/2}$ component of 2.06 eV, 1.87 eV, 1.69 eV and 1.2 eV were shown to correspond to surface atoms with coordination numbers 7, 8 and 9 and to Yb atoms in the bulk with coordination number 12 respectively. All these values are considerably larger than those observed in the $(\sqrt{5}\times\sqrt{5})R26.6°$- and $c(2\times2)$-Yb/Al(001) structures. This observation and the similarity with the energy position of the surface peaks in $YbAl_3$ and $YbAl_2$ are clearly consistent with the structural results discussed above which show that the Yb atoms are well embedded into the Al surface in these two phases.

At a coverage of 0.5 ML the first Yb layer is completed, and for higher coverages the doublet B with the $4f_{7/2}$ component at 0.12 eV below the Fermi level gradually grows in the spectra. The angle-resolved He I and He II spectra taken with a sample of coverage 0.6 ML are shown in Fig. 7a and Fig. 7b respectively for three different polar emission angles. The energy position of the component B is indicated. It can be seen in Fig. 7a that this component has higher relative intensity at normal emission than at grazing emission, which means that it is not due to a surface species but rather due to buried Yb. Furthermore, the energy position of 0.12 eV of this component is close to the 0.24 eV determined for the mixed-valence bulk Yb atoms in $YbAl_3$ and $YbAl_2$ [7], which gives further evidence that it can be assigned to mixed-valence Yb atoms embedded in Al. The fact that the spectrum in Fig. 6h is very similar to the one obtained from $YbAl_3$ [8] indicates that a local structure similar to $YbAl_3$ nucleates for coverages higher than 0.5 ML.

The He II spectra from the 0.6 ML sample taken at different emission angles are shown on a wider energy scale in Fig. 7b. Again, the energy positions of the doublet B arising from the $YbAl_3$-like nuclei are indicated by arrows. Furthermore, a broad structure between 4 eV and 10 eV is seen in these spectra. From the intensity variation of this feature with emission angle it can be concluded that it is, at least partly, connected with subsurface emitters as well. In $YbAl_3$ and $YbAl_2$ the bulk Yb atoms are in a mixed-valence state which gives rise to the characteristic $4f^{13}$ multiplet between 4 eV and 11 eV binding energy [7,8]. This multiplet structure, however, is blurred out in these spectra, which might be due to the fact that it overlaps with electron energy loss peaks: for Yb/Al(110), a band transition at 4.2 eV, a broad collective excitation at 8.6 eV and an interface plasmon at 12.4 eV have been reported by Onsgaard et al. [19].

The doublet C with the Yb $4f_{7/2}$ peak at 1.22 eV binding energy (Fig. 6h) has only little intensity for coverages below 1 ML; it is, however, recognized by the asymmetric tails of the components A in spectra of Fig. 6e–g for coverages above 0.5 ML. Its binding energy is very close to the one determined for the divalent surface Yb atoms in $YbAl_3$ and $YbAl_2$, and it can, therefore, be assigned to the topmost Yb atoms of the growing

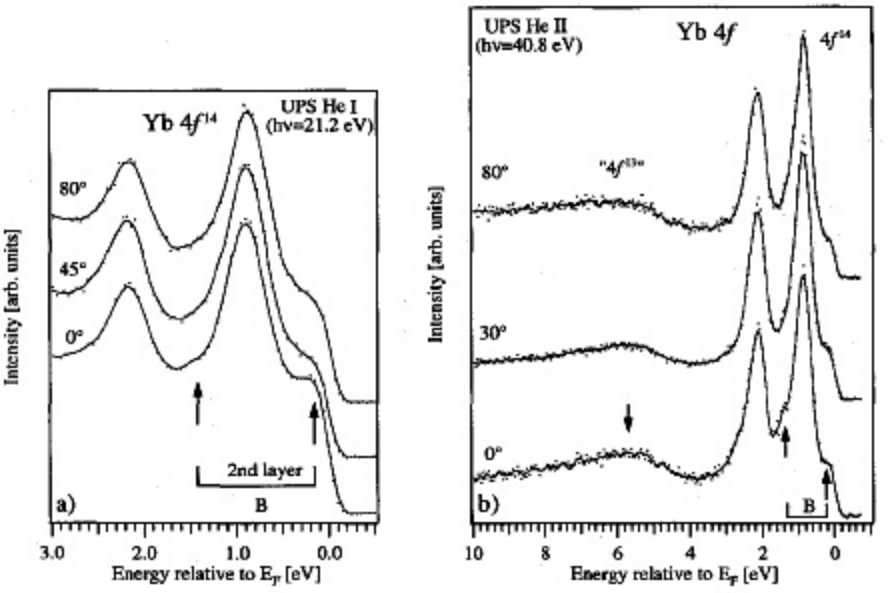

Fig. 7. Angle-resolved valence-band photoelectron spectra from 0.6 ML Yb/Al(001) for different polar emission angles with respect to the surface normal. In the He I spectra (a) the weak shoulders B indicated by the arrows are seen to be more intense at normal emission than at grazing emission, which indicates that they are due to subsurface emitters. As discussed in the text, the same conclusion holds for the broad "$4f^{13}$" feature between 4 eV and 10 eV in the He II spectra (b).

$YbAl_3$-like nuclei. From the fact that this component C already appears at coverages below 1 ML, it can be concluded that after completion of the $c(2\times2)$ layer the growth of Yb on Al(001) deviates substantially from a simple layer-by-layer growth.

3.2.2. The Al sp surface state

In Fig. 6a, the spectrum from the 0.2 ML $(\sqrt{5}\times\sqrt{5})R26.6°$ structure has an additional peak labeled S at a binding energy of 2.88 eV. This peak is already suppressed strongly and shifted slightly towards lower binding energies in Fig. 6b from the 0.25 ML sample. The origin of this peak can be found by a comparison of Fig. 6a with the corresponding spectrum from the clean Al(001) surface (Fig. 8). The spectra shown in Fig. 8 have been measured at normal emission and with an angular resolution of $\pm1°$. The Al(001) spectrum (Fig. 8a) is dominated by the well-known sp surface state [22] at 2.75 eV binding energy. The peak labeled S in the spectrum from the $(\sqrt{5}\times\sqrt{5})R26.6°$ sample (Fig. 8b) appears at 0.13 eV higher binding energy. If this peak is derived from the Al surface

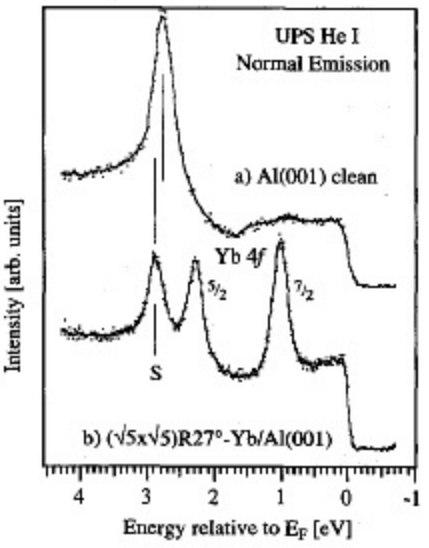

Fig. 8. Angle-resolved valence-band photoelectron spectra from (a) clean Al(001) and (b) $(\sqrt{5}\times\sqrt{5})R26.6°$-Yb/Al(001). The peak labeled S at 2.88 eV binding energy appears close to the zone-center sp surface state of the clean Al(001) surface.

state rather than being due to a Yb core state, it is expected to disperse as a function of parallel momentum. A series of energy spectra measured along the [100] azimuth ($\bar{\Gamma}\bar{M}$) and the [110] azimuth ($\bar{\Gamma}\bar{X}$) is shown for clean Al(001) and for $(\sqrt{5}\times\sqrt{5})$R26.6°-Yb/Al(001) in Fig. 9a and Fig. 9b respectively. In Fig. 9a, the free-electron-like Al(001) surface state and two bands due to bulk transitions are indicated. In Fig. 9b, the Yb 4f doublet shows up as two horizontal dark lines separated by the spin–orbit splitting of 1.27 eV. At $\bar{\Gamma}$ the peak labeled S is recognized at 2.88 eV below the Fermi level. Even though its intensity becomes rather weak with increasing polar emission angle, it is clearly seen to disperse towards the Fermi level, similar to the clean surface state in Fig. 9a.

It has been shown [23] that Na adsorption on Al(001) strongly modifies the surface electronic structure. For room-temperature adsorption where the Na atoms occupy substitutional sites, a 0.45 eV shift of the Al sp surface state towards lower binding energies and a strongly modified dispersion has been found. Given the strong reconstruction and the large vibrational amplitudes of the first substrate layer in the $(\sqrt{5}\times\sqrt{5})$R26.6°-Yb/Al(001) structure [18], it is, therefore, very unlikely that this structure can support a surface state with an energy at $\bar{\Gamma}$ as close as 0.13 eV to the surface state of the clean Al(001) surface and of comparable peak width. Furthermore, an intrinsic surface state of the $(\sqrt{5}\times\sqrt{5})$R26.6° phase is expected to show dispersion according to the $(\sqrt{5}\times\sqrt{5})$R26.6° periodicity, which is not observed in the present case. Therefore, the most natural explanation for the existence of this state on the 0.2 ML Yb/Al(001) surface is that it originates from unreconstructed surface patches containing second-layer Yb atoms, as is discussed in Ref. [18]. The observed energy shift of 0.13 eV might be due to the presence of Yb atoms below the surface which modify the bonding of the surface Al atoms. Alternatively, it could be imagined that the observed surface state originates from the second substrate layer where the electrons are confined between the bulk and the strongly reconstructed and poorly commensurate topmost Yb–Al layer. Even though a clear-cut assignment of the origin of this state cannot be made at this time, it is clear from its dispersion behavior, and from the

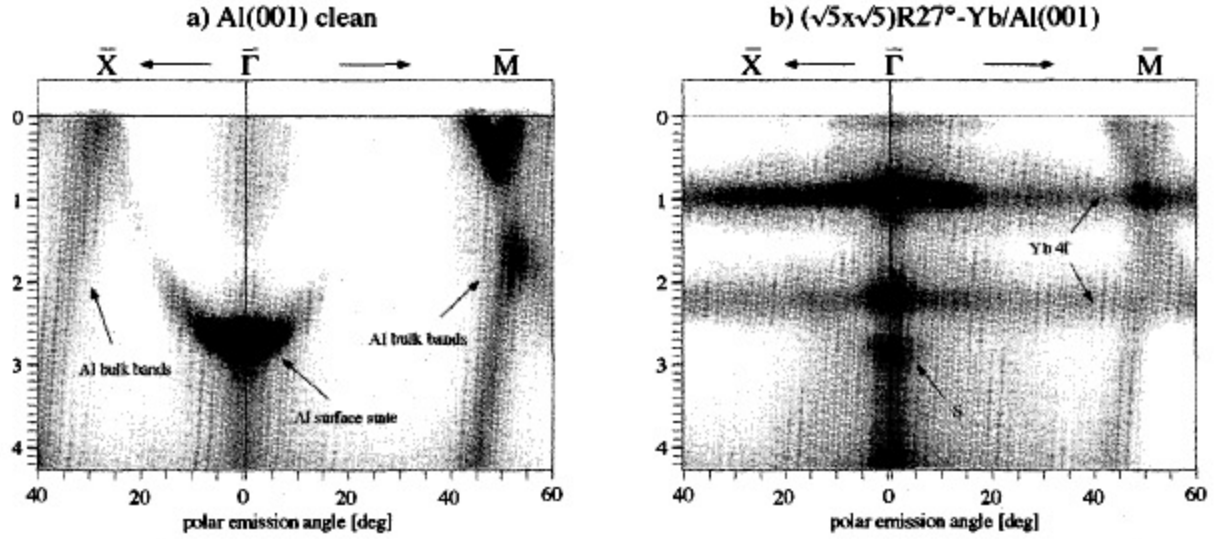

Fig. 9. Dispersion plots for (a) Al(001) and for (b) $(\sqrt{5}\times\sqrt{5})$R27°-Yb/Al(001) representing the photoelectron intensity between the Fermi level and 4.3 eV binding energy for polar emission angles along the [100] azimuth ($\bar{\Gamma}\bar{M}$) and the [110] azimuth ($\bar{\Gamma}\bar{X}$). Intensities are given in a linear gray scale with low intensities in white and high intensities in black. Prominent features are indicated by arrows. The peak labeled S is clearly seen to disperse towards the Fermi level, even though its intensity becomes rather weak with increasing polar emission angle.

fact that it is observed at the same energy location with He I and He II radiation (not shown), that it has extended two-dimensional character and must be due to the surface.

One further intriguing observation can be made by a comparison of the plots in Fig. 9a and b. In the plot for the clean Al(001) surface (Fig. 9a), a band due to bulk transitions is observed to disperse from about 4 eV at 40° polar emission angle ($\bar{\Gamma}\bar{X}$ direction) towards the Fermi level, which is crossed at about 28° polar emission angle. In the plot for the $(\sqrt{5}\times\sqrt{5})$R26.6°-Yb/Al(001) surface, this band has completely disappeared. The Al bulk band under question shows relatively high intensity at the Fermi level crossing, and it should, therefore, leave a clear signature on the Al(001) Fermi energy map [24]. The Fermi energy maps from clean Al(001) and from $(\sqrt{5}\times\sqrt{5})$R26.6°-Yb/Al(001) are given in Fig. 10. These maps represent the intensity of the photoelectrons emitted from the Fermi edge as a function of emission angle and thus as a function of parallel momentum $k_{\parallel}$. In the upper right half of the clean Al(001) Fermi energy map (Fig. 10a) the projection of the bulk Brillouin zone is indicated by continuous black lines, and the boundary of the surface Brillouin zone is given by straight dashed lines. The dashed half-circle indicates the location of the sp surface state, which appears as a weak circular contour touching a bulk band close to the $\bar{X}$ point. The features in the Al(001) Fermi energy map due to the Fermi level crossings of the two bulk bands observed in Fig. 9a can easily be made out. The date-shaped strong maxima located at the four $\bar{M}$ points are due to the bulk band seen in the right half of Fig. 9a, whereas the intensity enhancement around the $\bar{X}$ points stems from the band observed in the left half of Fig. 9a which has disappeared in the plot for $(\sqrt{5}\times\sqrt{5})$R26.6°-Yb/Al(001) (Fig. 9b). In fact, the most striking difference of the Fermi energy map from $(\sqrt{5}\times\sqrt{5})$R26.6°-Yb/Al(001) shown in Fig. 10b is that the intensity at the $\bar{X}$ points is suppressed strongly, as is also the intensity of the arc-shaped contours crossing the $\bar{X}$ points and passing close to the $\bar{M}$ points.

This suppression of bulk transitions due to adsorbate-induced surface reconstruction is very unexpected and, to our knowledge, has not previously been observed. It poses several questions. How far does the influence of the $(\sqrt{5}\times\sqrt{5})$

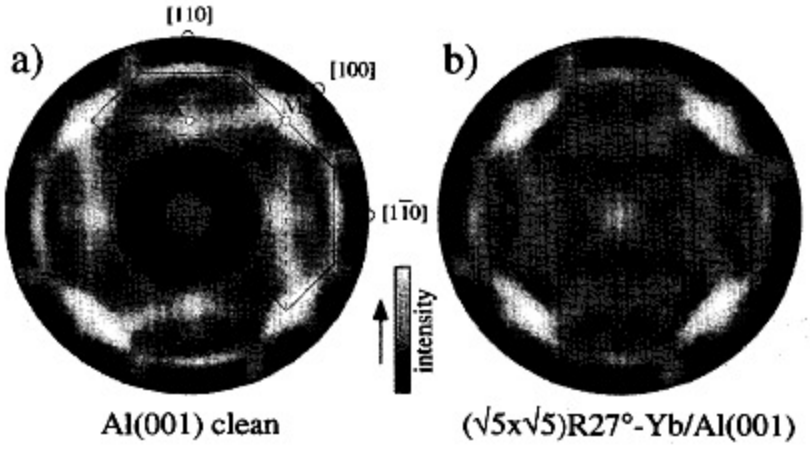

Fig. 10. Fermi energy maps from (a) clean Al(001) and (b) $(\sqrt{5}\times\sqrt{5})$R26.6°-Yb/Al(001). These maps represent the intensity of the photoelectrons emitted from the Fermi edge as a function of emission angle and thus as a function of parallel momentum $k_{\parallel}$. The intensities are given in a linear gray scale with low intensity corresponding to black and high intensity corresponding to white. In the upper right half of (a) the projection of the bulk Brillouin zone is indicated by continuous black lines, and the boundary of the surface Brillouin zone is given by straight dashed lines. The dashed half-circle indicates the location of the sp surface state (Fig. 9a), which appears as a weak circular contour touching a bulk band close to the $\bar{X}$ point. The most striking difference between the Fermi energy map from Al(001) (a) and from $(\sqrt{5}\times\sqrt{5})$R26.6°-Yb/Al(001) (b) is that the intensity at the $\bar{X}$ points and the intensity of the arc-shaped contours crossing the $\bar{X}$ points and passing close to the $\bar{M}$ points is suppressed strongly.

R26.6° surface reconstruction on the electronic levels reach into the substrate? Are the electronic states of this band so strongly coupled to the surface that the change in periodicity upon reconstruction inhibits their survival? Or, is the apparent suppression of these bulk transitions a final state rather than an initial state effect, due to modified coupling of the inverse LEED-type state of the outgoing electron at the reconstructed surface? In order to understand the underlying mechanisms, the nature of the bulk transitions under consideration would have to be properly determined, which could be done using an appropriate calculation scheme. Work along these lines is planned.

4. Conclusions

The structural phases upon formation of the Yb/Al(001) interface have been characterized by LEED, XPD and UPS. Two long-range ordered reconstructions are found to form at 0.2 ML and 0.5 ML Yb coverage, which coexist with surface patches containing mixed-valence second-layer Yb atoms. A discontinuous structural transition is observed between 0.2 ML and 0.25 ML Yb coverage, which is attributed to a collective rearrangement of the Yb atoms into a regular array of $c(2\times2)$ nuclei. Between 0.25 ML and 0.5 ML these $c(2\times2)$ nuclei grow in size continuously, and a well-ordered $c(2\times2)$ structure is observed at 0.5 ML coverage. The changes in local environment due to these structural transitions are clearly reflected in the Yb 4f core-level spectra. In contrast to findings for Sm adsorbed on Pd(100), Cu(100) and Al(001), where the Sm valency has been found to be strongly coverage dependent [25], it is found that the surface Yb atoms on Al(001) remain in the divalent $4f^{14}$ state up to the completion of the first layer which occurs at 0.5 ML coverage. For higher coverages a valence transition of the Yb atoms incorporated into growing $YbAl_3$-like nuclei is observed. Diffusion of Yb into the Al substrate is found to occur as a two-step process. A slow diffusion is observed at temperatures slightly above room temperature, and a strongly enhanced diffusion for temperatures above 140°C. It is proposed that the initially slow diffusion is due to the considerable energy difference between the valence states of Yb adsorbed on the surface and of Yb in Al. For initial coverages higher than 0.2 ML a stable divalent $(\sqrt{5}\times\sqrt{5})$R26.6° surface layer is always obtained upon annealing above 200°C. Surprisingly, this reconstructed surface layer is found to suppress Al bulk transitions in the vicinity of the $\bar{X}$ point of the surface Brillouin zone. Furthermore, a zone-center surface state similar to the well-known sp surface state of the clean Al(001) surface is observed in the 0.2 ML $(\sqrt{5}\times\sqrt{5})$R26.6° phase.

Acknowledgements

We thank T. Greber for many stimulating discussions and for a critical reading of the manuscript. One of us (P.A.) is grateful for support by the "Profil-Stipendium" of the Fonds National Suisse pour la Recherche Scientifique. Skillful technical assistance was provided by E. Mooser, O. Raetzo, F. Bourqui, and H. Tschopp. This project has been supported by the Fonds National Suisse pour la Recherche Scientifique.

References

[1] P. Wachter, H. Boppart (Eds.), Valence Instabilities, North-Holland, Amsterdam, 1982.
[2] W.-D. Schneider, C. Laubschat, B. Reihl, Phys. Rev. B 27 (1983) 6538.
[3] M. Domke, C. Laubschat, M. Prietsch, T. Mandel, G. Kaindl, W.-D. Schneider, Phys. Rev. Lett. 56 (1986) 1287.
[4] A. Stenborg, J.N. Andersen, O. Björneholm, A. Nilsson, N. Mårtensson, Phys. Rev. Lett. 63 (1989) 187.
[5] E.E. Havinga, K.H.J. Buschow, H.J. van Daal, Solid State Commun. 13 (1973) 621.
[6] F. Patthey, J.-M. Imer, W.-D. Schneider, Y. Baer, B. Delley, F. Hulliger, Phys. Rev. B 36 (1987) 7697.
[7] G. Kaindl, B. Reihl, D.E. Eastman, R.A. Pollak, N. Mårtensson, B. Barbara, T. Penney, T.S. Plaskett, Solid State Commun. 41 (1982) 157.
[8] S.-J. Oh, S. Suga, A. Kakizaki, M. Taniguchi, T. Ishii, J.-S. Kang, J.W. Allen, O. Gunnarsson, N.E. Christensen, A. Fujimori, T. Suzuki, T. Kasuya, T. Miyahara, H. Kato, K. Schönhammer, M.S. Torikachvili, M.B. Maple, Phys. Rev. B 37 (1988) 2861.
[9] G.G. Tibbetts, W.F. Egelhoff, Jr., J. Vac. Sci. Technol. 17 (1980) 458.

[10] R. Nyholm, I. Chorkendorff, J. Schmidt-May, Surf. Sci. 143 (1984) 177.
[11] T. Greber, J. Osterwalder, L. Schlapbach, Phys. Rev. B 40 (1989) 9948.
[12] W.P. Ellis, in: H. Lipson (Ed.), Optical Transforms, Academic Press, London, 1972.
[13] C.S. Fadley, in: S.G. Davison (Ed.), Progress in Surface Science, Pergamon, New York, 1984, Vol. 16, p. 275. C.S. Fadley, in: R.Z. Bachrach (Ed.), Synchrotron Radiation Research: Advances in Surface Science, Plenum, New York, 1990, Chapter 11.
[14] R. Fasel, P. Aebi, L. Schlapbach, J. Osterwalder, Phys. Rev. B 52 (1995) R2313.
[15] J. Osterwalder, P. Aebi, R. Fasel, D. Naumovic, P. Schwaller, T. Kreutz, L. Schlapbach, T. Abukawa, S. Kono, Surf. Sci. 331–333 (1995) 1002.
[16] R. Fasel, J. Osterwalder, Surf. Rev. Lett. 2 (1995) 359.
[17] R. Fasel, P. Aebi, J. Osterwalder, L. Schlapbach, Surf. Sci. 331 (1995) 80.
[18] R. Fasel, M. Gierer, H. Bludau, P. Aebi, J. Osterwalder, L. Schlapbach, Surf. Sci. 374 (1997) 104.
[19] J. Onsgaard, I. Chorkendorff, O. Ellegaard, O. Sørensen, Surf. Sci. 138 (1984) 148.
[20] R. Fasel, P. Aebi, T. Greber, J. Osterwalder, L. Schlapbach, Surf. Rev. Lett. in press.
[21] I. Chorkendorff, J. Kofoed, J. Onsgaard, Surf. Sci. 152–153 (1985) 749.
[22] P.O. Gartland B.J. Slagsvold, Solid State Commun. 25 (1978) 489. G.V. Hansson, S.A. Flodstrom, Phys. Rev. B 18 (1978) 1562.
[23] R. Fasel, P. Aebi, R.G. Agostino, L. Schlapbach, J. Osterwalder, Phys. Rev. B 54 (1996) 5893.
[24] P. Aebi, J. Osterwalder, R. Fasel, D. Naumovic, L. Schlapbach, Surf. Sci. 307–309 (1994) 917.
[25] Å. Fäldt, H.P. Myers, Phys. Rev. B 37 (1988) 2682, and references cited therein.